symmetry

IMPACT FACTOR 2.2

CITESCORE 5.4

Article

Stability Analysis of Stable Circular Orbit in Multi-Static Black Hole Spacetime

Zefang Fan, Yu Wang and Xianggao Wang

MDPI

https://doi.org/10.3390/sym16091140

symmetry

MDPI

Article

Stability Analysis of Stable Circular Orbit in Multi-Static Black Hole Spacetime

Zefang Fan, Yu Wang * and Xianggao Wang

Guangxi Key Laboratory for Relativistic Astrophysics, School of Physical Science and Technology, Guangxi University, Nanning 530004, China; 2307301022@st.gxu.edu.cn (Z.F.); wangxg@gxu.edu.cn (X.W.)
* Correspondence: 2107401023@st.gxu.edu.cn

Abstract: We herein study the circular orbit stability of a static black hole system composed of multiple Reissner–Nordstrom (RN) black holes. By comparing the circular orbits of two static black holes, three static black holes (TBHs), four static black holes and five static black holes at different spacetime, we find that the continuity of their stable circular orbits changes, i.e., the peaks of the effective potentials are transformed from single-peaked to bi-peaked, and that the distance a between the black holes is the main reason for this change. This characteristic is completely different from the continuity of the stable circular orbit interval of any kind of single black hole in the past. After calculation, we obtain several critical values that lead to the change in circular orbit stability. The three fundamental frequencies (orbital frequency, radial local frequency, and vertical local frequency) are derived and compared for two different spacetimes of double and three black holes. We also analyse the effect of the black hole distance *a* on the three fundamental frequencies of circular orbits.

Keywords: effective potential; RN black holes; ISCO; three frequencies

check for updates

Citation: Fan, Z.; Wang, Y.; Wang, X. Stability Analysis of Stable Circular Orbit in Multi-Static Black Hole Spacetime. *Symmetry* **2024**, *16*, 1140. https://doi.org/10.3390/sym16091140

Academic Editors: Charalampos Moustakidis and Stefano Profumo

Received: 31 May 2024
Revised: 1 August 2024
Accepted: 6 August 2024
Published: 3 September 2024

1. Introduction

A hundred years ago, Einstein predicted the existence of gravitational waves; however, it has been difficult to confirm them for a long time. Most local galaxies, nearly all of them, are thought to harbour a massive black hole at their centre. Theoretically, black holes, neutron stars, and other celestial bodies are capable of colliding and merging to produce gravitational waves [1]. Since 2015, scientists have detected ten gravitational waves resulting from the mergers of black holes, as well as one produced by the collision of two neutron stars [2,3]. The discovery of gravitational waves has greatly advanced the study of phenomena around binary black hole systems [4].

Scientists have also discovered a mysterious black hole phenomenon, which is that three black holes are attracted to each other, in a situation that is about to merge [5,6]. These three black holes are all supermassive black holes; if they merge, they will produce a huge amount of energy, this discovery is very important for scientists. Research utilising the Sloan Digital Sky Survey (SDSS) data reveals that approximately 0.2 percent of merging systems feature three galaxies [7]. The galaxy SDSS J0849+1114 has been identified as the first discovered triple type 2 Seyfert nucleus. The scientists made the breakthrough using the Dual Imaging Spectrograph on the 3.5-metre telescope at Cape Apache Observatory [8,9]. Therefore, scientists estimate that this newly formed galaxy must be hiding many secrets. One of the most obvious findings is that there is more than one supermassive black hole in this galaxy, and they are rapidly accumulating matter, which is why the anomalous data appear [10]. It is believed that analogous configurations were more prevalent in the primordial cosmos, a time when the collision of galaxies was considered to occur at a higher rate [11,12]. Therefore, the study of multi-static black hole systems is of great significance for us to reveal the laws of the Universe, and it hints at its future impact.

Investigating the dynamics of particles under intense gravitational forces is of paramount significance, both within the domains of astrophysics and the framework of gravitational

theory. This challenge continues to be one of the most fundamental issues within the context of multi-static black hole systems. Certainly, the emergence of the three black hole shadows referred to is contingent upon the dynamics of particles lacking mass [13]. Alternatively, the behaviour of massive particles within binary black hole systems has been examined in relation to gravitational wave emissions triggered by the influence of a third body [14–17] and the emergence of several accretion disks [18,19]. In these scenarios, the preservation of stable circular orbits is essential, with the innermost stable circular orbit (ISCO) being especially significant [20,21].

Binary black hole systems scattered throughout the Universe are multifaceted and of ever-changing complexity. Numerical relativity methods, if utilised, can be of great benefit in explaining the phenomena occurring in these complex systems. In addition, the use of analytical techniques is essential to obtain a qualitative understanding of these phenomena. Therefore, we usually use a static and axisymmetric dihole spacetime as a simplified model [22]. There are some dihole solutions of Einstein's equations with these symmetries, such as the Weyl spacetime [23], the Majumdar–Papapetrou (MP) spacetime [24,25], and the two-Kerr spacetime [26]. Studying such a spacetime phenomenon can provide us with valuable insights and strong indications for multi-static black hole occurrences, enhancing our understanding of the multi-static black hole issue.

Numerous studies have explored the stability of circular orbits around static black holes, yet the objective of this paper is to clarify the properties of stable circular orbits within environments containing multiple black holes [4,27–33]. We conduct a comparative study of the circular orbits in systems involving a single black hole, two static black holes, and progress to systems with three, four, and five static black holes across five different spacetime scenarios. A particularly intriguing aspect of this research is the investigation into how the continuity of the innermost stable circular orbits in multi-black hole configurations alters. To achieve this, we delve into the stable circular orbits along the axis of symmetry in a dihole system, which is situated in a spacetime hosting two equal-mass TBHs—an exact solution to the Einstein–Maxwell equations and comprising two extreme RN black holes. We predict that with changes in 'a', the peak of the effective potential that determines stable circular orbits may evolve a shift from a single peak to a bimodal form. Previous research has indicated that the stable circular orbits in the MP dihole spacetime exhibit a range of behaviours. For instance, the stability of orbits for massive particles is not uniform, and stable photon orbits can be found within regions that are otherwise unstable. These findings are also relevant to the TBH spacetime [34,35].

This paper focuses on analysing the dependence of the sequence of stable circular orbits on the separation distance. Firstly, we divide the parameter range, at each boundary of which the stabilising circular orbits are discontinuous. Further, we analyse the one-dimensional effective potential of spacetime. Finally, we also analyse the effect of the multiple black hole spacing a on the three fundamental frequencies of circular orbits (orbital frequency, radial local frequency, and vertical local frequency). It is important to note that the effect on the frequencies is similar to that of stabilising circular orbits. Therefore, ISCO represents a circular orbit stabilised with a minimum radius. We find that the position of the ISCO becomes discontinuous at a certain distance and obtain a figure of ISCO for different black hole spacetime.

The structure of this paper is organised as follows: Section 2 outlines the spacetime metric and the equations of motion for black holes. Section 3 examines the stability of circular orbits within a multi-static black hole spacetime, using the example of a three-black hole system. Section 4 delves into the one-dimensional effective potentials for spacetime containing two and three black holes. In Section 5, we calculate the three fundamental frequencies (orbital frequency, radial local frequency, and vertical local frequency) for circular orbits in a multi-static black hole environment, discovering that when the black hole separation distance a approaches zero, the outcomes resemble those of the Schwarzschild black hole [36]. The paper concludes with Section 6, which offers a summary and discussion of the findings. Throughout the paper, we adopt the units where G = 1 and c = 1.

2. Multi-Static Black Hole Spacetime Metric and Equations of Motion

The metric of spacetime encodes essential information about it, and our investigation starts with the genesis of multi-static black holes. The MP spacetime metric is expressed as follows:

$$ds^2 = -U^{-2}(\vec{r})dt^2 + U^2(\vec{r})d\vec{r} \cdot d\vec{r}, \tag{1}$$

where

$$d\vec{r} \cdot d\vec{r} = dx^2 + dy^2 + dz^2, \tag{2}$$

while

$$R_{\mu\nu} - \frac{1}{2}g_{\mu\nu}R = \kappa T_{\mu\nu}. \tag{3}$$

We set $T_{\mu\nu} = 0$. The quantity U in this context satisfies the Einstein field Equation (3), which can be directly simplified to the Laplace Equation (4).

$$\bigtriangledown^2 U = \frac{\partial^2 U}{\partial x^2} + \frac{\partial^2 U}{\partial y^2} + \frac{\partial^2 U}{\partial z^2} = 0. \tag{4}$$

The pertinent solution was provided in Hawking's publication [37]:

$$U(x) = 1 + \sum_i \frac{m_i}{r_i}, \tag{5}$$

$$r_i = \left[(x - x_i)^2 + (y - y_i)^2 + (z - z_i)^2\right]^{\frac{1}{2}}. \tag{6}$$

This U is analogous to a gravitational potential, where i moves from 1 to 3. In this context, $\vec{r}$ denotes the vector that indicates the position within the plane of a three-dimensional space, known as the background space. The schematic diagram of the static linear triple black hole system studied in this paper is shown in Figure 1.

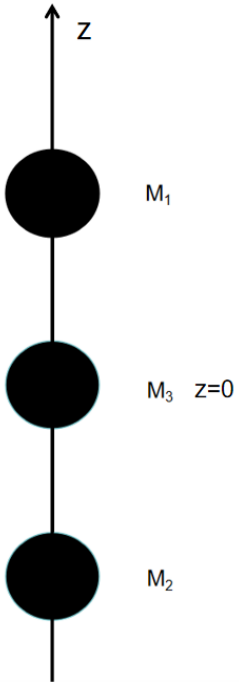

Figure 1. Static linear triple black hole schematic diagram.

We focus on the spacetime properties of static linear triple black holes and give the metric and canonical fields of the TBH spacetime in the following isotropic coordinate system:

$$ds^2 = g_{\mu\nu}dx^\mu dx^\nu = \frac{-dt^2}{U^2} + U^2(d\rho^2 + \rho^2 d\phi^2 + dz^2). \tag{7}$$

In order to simplify subsequent computations, the covariant elements of the metric tensor are expressed as follows:

$$g_{tt} = -U^{-2}, \tag{8}$$

$$g_{\rho\rho} = U^2, \tag{9}$$

$$g_{\phi\phi} = U^2\rho^2, \tag{10}$$

$$g_{zz} = U^2, \tag{11}$$

$$A_\mu dx^\mu = A^\nu g_{\mu\nu}dx^\mu = \Phi U^{-2}dt = U^{-1}dt, \tag{12}$$

$$\Phi(\vec{r}) = U(\vec{r}). \tag{13}$$

Equation (13) can be introduced through Equation (12). Equation (13) indicates that the electrostatic potential is equivalent to the gravitational potential. In a spacetime governed by this equation, black holes can exist at various positions. If these black holes possess identical charges, they can maintain a state of mutual static equilibrium, which gives rise to a static spacetime. After a transformation of coordinates, we obtain the explicit representation of U in cylindrical coordinate systems:

$$U(\rho, z) = 1 + \frac{M_1}{\sqrt{\rho^2 + (z-a)^2}} + \frac{M_2}{\sqrt{\rho^2 + (z+a)^2}} + \frac{M_3}{\sqrt{\rho^2 + z^2}}. \tag{14}$$

In the context of this discussion, M_i $(i = 1, 2, 3)$ denotes the masses of three extreme RN black holes. The masses M_1 and M_2 are positioned at $z = \pm a$ (with $a \geq 0$), while M_3 is situated at $z = 0$. It is important to note that we employ cylindrical coordinates in the spatial geometry, defined as $x = \rho\cos\phi$ and $y = \rho\sin\varphi$, where x and y correspond to the Cartesian coordinates.

Using this analogy, it becomes evident that the Lagrangian for freely falling particles in curved spacetime is as follows:

$$\mathcal{L} = \frac{1}{2}g_{\mu\nu}\dot{x}^\mu\dot{x}^\nu = \frac{1}{2}\left[-\frac{\dot{t}^2}{U^2} + U^2\left(\dot{\rho}^2 + \rho^2\dot{\phi}^2 + \dot{z}^2\right)\right]. \tag{15}$$

The key aspect is the derivative with respect to the affine parameter. Given that the TBH spacetime is static and axisymmetric, the variables t and the angular coordinate ϕ do not appear explicitly in the Lagrangian, leading to the conservation of energy and angular momentum. Observe that the conserved quantity corresponds to a specific component of the covariant quantity. Upon returning to the TBH spacetime, it is straightforward to observe that the coordinates t and ϕ are cyclic, implying that the conserved quantities for the moving particles are the momenta p_t and p_ϕ.

$$E = \frac{\dot{t}}{U^2}, \quad L = \rho^2 U^2\dot{\phi}. \tag{16}$$

We can assume that the energy E is positive. The Euler–Lagrangian equation is

$$\frac{d}{dt}\frac{\partial L}{\partial \dot{q}_\alpha} - \frac{\partial L}{\partial q_\alpha} = 0. \tag{17}$$

We can now derive the equations of motion for z and ρ in four-dimensional spacetime coordinates by employing the Lagrange equation, as depicted below:

$$U^2\ddot{z} - [\dot{t}^2 U^{-3} + U(\dot{\rho}^2 + \rho^2\dot{\phi}^2 + \dot{z}^2)]U_z = 0, \tag{18}$$

$$U^2\ddot{\rho} - [U^2\dot{\phi}^2\rho + (U^{-3}\dot{t}^2 + U(\dot{\rho}^2 + \rho^2\dot{\phi}^2 + \dot{z}^2))U_\rho] = 0, \tag{19}$$

where the partial derivatives of the potential energy function U with respect to the coordinates z and ρ are denoted as U_z and U_ρ, respectively.

3. Stability Conditions for Circular Orbits in Multi-Static Black Hole Spacetime

Let us take TBHs as an example. In order to simplify the calculations, we examine time-like particles that orbit in a circle on a symmetric plane, which must adhere to these conditions: $z = 0$. The radius and ordinate of the particle's circular orbit remain constant over proper time, with $\dot{\rho} = \dot{z} = 0$. Clearly, the acceleration terms must also equal to zero, $\ddot{\rho} = \ddot{z} = 0$. From this, we can deduce the following:

$$V_z = 0, \tag{20}$$

$$V_\rho = 0, \tag{21}$$

where $V_i = \partial_i V$ for $i = z, \rho$. Consequently, circular orbits are achieved at the stationary points of V, where the values of V are positive. After simplification, we obtain the following equations:

$$U_z = 0, \tag{22}$$

$$U_\rho = -\frac{\rho}{(\rho^2 + z^2)^{\frac{3}{2}}} - \frac{\rho}{(\rho^2 + (z-a)^2)^{\frac{3}{2}}} - \frac{\rho}{(\rho^2 + (z+a)^2)^{\frac{3}{2}}}. \tag{23}$$

$$L^2 = L_0^2(\rho, z) := -\frac{\rho^3 U^2 U_\rho}{U + 2\rho U_\rho}. \tag{24}$$

$$E^2 = E_0^2(\rho, z) := V\left(\rho, z; L_0^2\right). \tag{25}$$

Equation (24) corresponds to the angular momentum of a particle in the class of circular orbits, while Equation (25) represents its associated energy. We stipulate that the square of the angular momentum must be greater than zero, which implies that the effective potential energy must also be greater than zero. Consequently, the particle's motion along the circular orbit must adhere to the following criteria: $U_z = 0$, $L^2 = L_0^2 \geq 0$, and $E^2 = E_0^2$. Next, we examine the stability of the circular orbit. Stability theory posits that a circular orbit is stable if the effective potential reaches a minimum at that orbit. Conversely, if the effective potential attains a local maximum or a saddle point, the orbit is considered unstable. To ascertain the stability of the circular orbit, we utilize the Hessian matrix, the elements of which are given as $V_{ij} = \partial_i \partial_j V$, and then we define the determinant and trace of the Hessian matrix:

$$h\left(\rho, z; L^2\right) = \det V_{ij} = V_{\rho\rho}V_{zz} - V_{\rho z}V_{z\rho}, \tag{26}$$

$$k\left(\rho, z; L^2\right) = \mathrm{Tr}\, V_{ij} = V_{\rho\rho} + V_{zz}. \tag{27}$$

We can summarize the stability analysis of circular orbits as follows: (1) A circular orbit is stable at a point of minimum potential V if and only if $h > 0$, $k > 0$. (2) A circular orbit is unstable at a point of minimum potential V if and only if $h > 0$, $k < 0$, or $h < 0$. As a sequence of stable circular orbits shifts to an unstable sequence at a particular radius, the circular orbit at this critical radius is termed an edge-stable circular orbit, and the potential V displays an inflection point (i.e., $h = 0$). Herein, we refer to the smallest edge-stable circular orbit as the ISCO. In the remainder of the article, we investigate the circular orbits of equal mass $M_1 = M_2 = M_3$ in the TBH spacetime. We employ units where $M_i = 1$ for $i = 1, 2, 3$.

We express the trace and determinant of the Hessian matrix for circular orbits in the following manner:

$$h_0(\rho, z) = h\left(\rho, z; L_0^2\right)\Big|_{U_z=0}, \tag{28}$$

$$k_0(\rho, z) = k\left(\rho, z; L_0^2\right)\Big|_{U_z=0}. \tag{29}$$

Based on this, we can deduce the domain of motion for the circular orbit in the given example:

$$D = \left\{(\rho, z)|h_0 > 0, k_0 > 0, L_0^2 > 0\right\}. \tag{30}$$

In the $z = 0$ plane, the marginally stable circular orbits satisfy the following conditions:

$$V_\rho = 0. \tag{31}$$

$$V_{\rho\rho} = 0. \tag{32}$$

By means of the system of joint equations, the edge-stabilised circular orbits and their angular momentum magnitudes corresponding to different a are solved, and the minimum value of the edge-stabilised circular orbit is the innermost stable circular orbit. We present the results in Table 1.

Table 1. The solution of equations, where $M_1 = M_2 = M_3 = M$.

a/M	j/M	ρ/M
3.00	3.57	1.31
2.09	4.47	0.96
2.09	7.96	5.11
2.09	7.96	5.24
1.50	5.28	0.82
1.50	9.45	2.67
1.50	8.20	11.48
1.09	8.08	0.65
1.09	1046136.59	1.61
1.09	8.34	8.29
0.85	56136.62	0.54
0.85	8.40	8.58
0.80	8.41	8.64
0.70	8.43	8.72
0.40	8.46	8.91
0	8.48	13.19

By calculation, we can discern that when a is greater than 2.09, the stable circular orbits are continuous, and this sequence can extend from the innermost stable circular orbit to infinity. However, when $a = 2.09$, the sequence of stable circular orbits is no longer continuous and will be interspersed with a sequence of unstable circular orbits ranging from a radius of 7.11 to 7.24, while when it is beyond 7.24, it is once again a sequence of stable circular orbits. When $a = 1.09$, angular momentum divergence occurs, which means that the edge-stabilised circular orbit at a radius of 1.61 will disappear. When a is less than 1.09, two sets of normal solutions appear. When $a = 0.85$, the angular momentum diverges again, indicating that the original innermost stable circular orbit, $\rho = 0.54$, is about to vanish. When a is less than 0.85, a set of normal solutions emerges, where the sequence of stable circular orbits is no longer interrupted. We have selected four values and depicted this region in Figure 2.

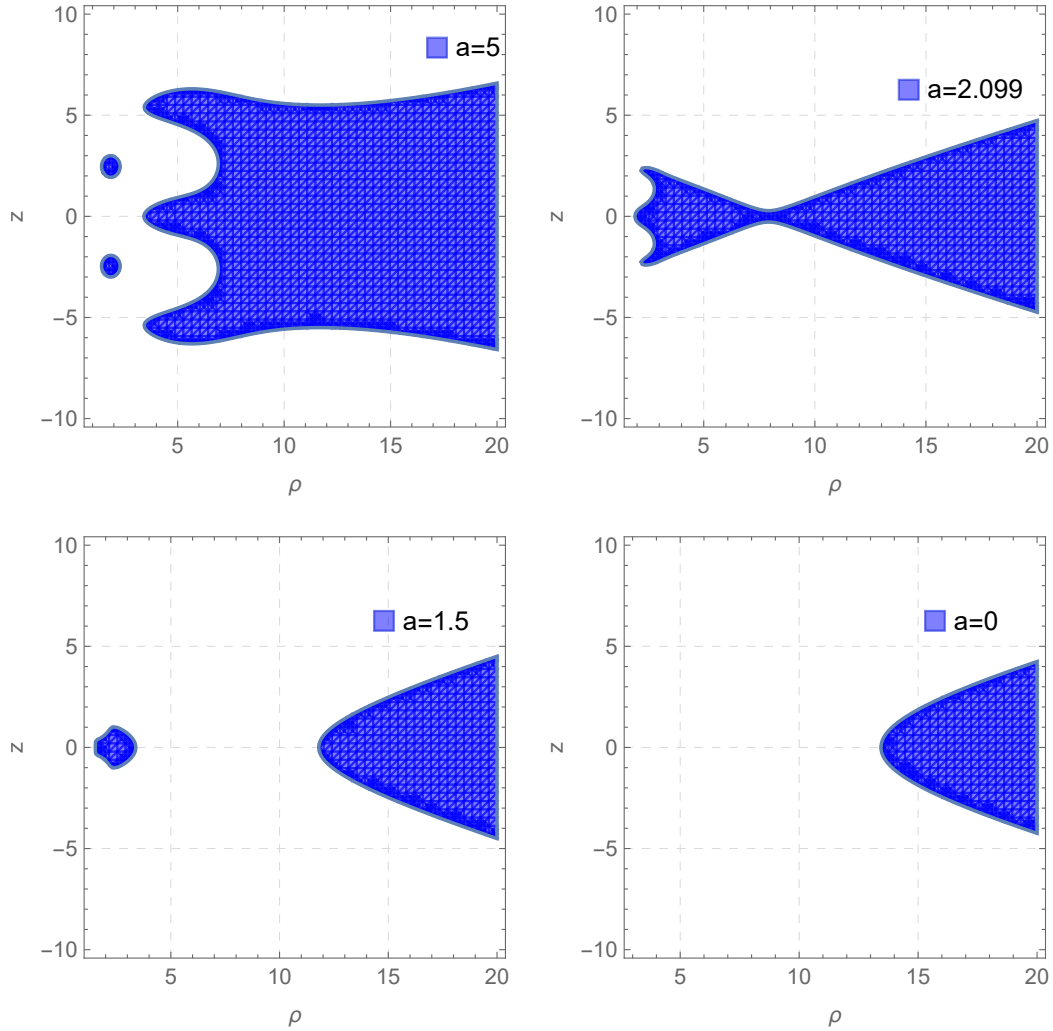

Figure 2. Figure of stabilised regions at different separation distances a.

Similarly, we have obtained a figure of stable circular orbital regions of other black hole spacetimes for further comparative analyses, as shown in Figure 3.

We have visualised the stability of the innermost circular orbits for systems with two, four, and five black holes. The stability of circular orbits varies across different spacetimes. This is intriguing, as we can clearly observe that the stability region's continuity shifts with the variation in the distance a.

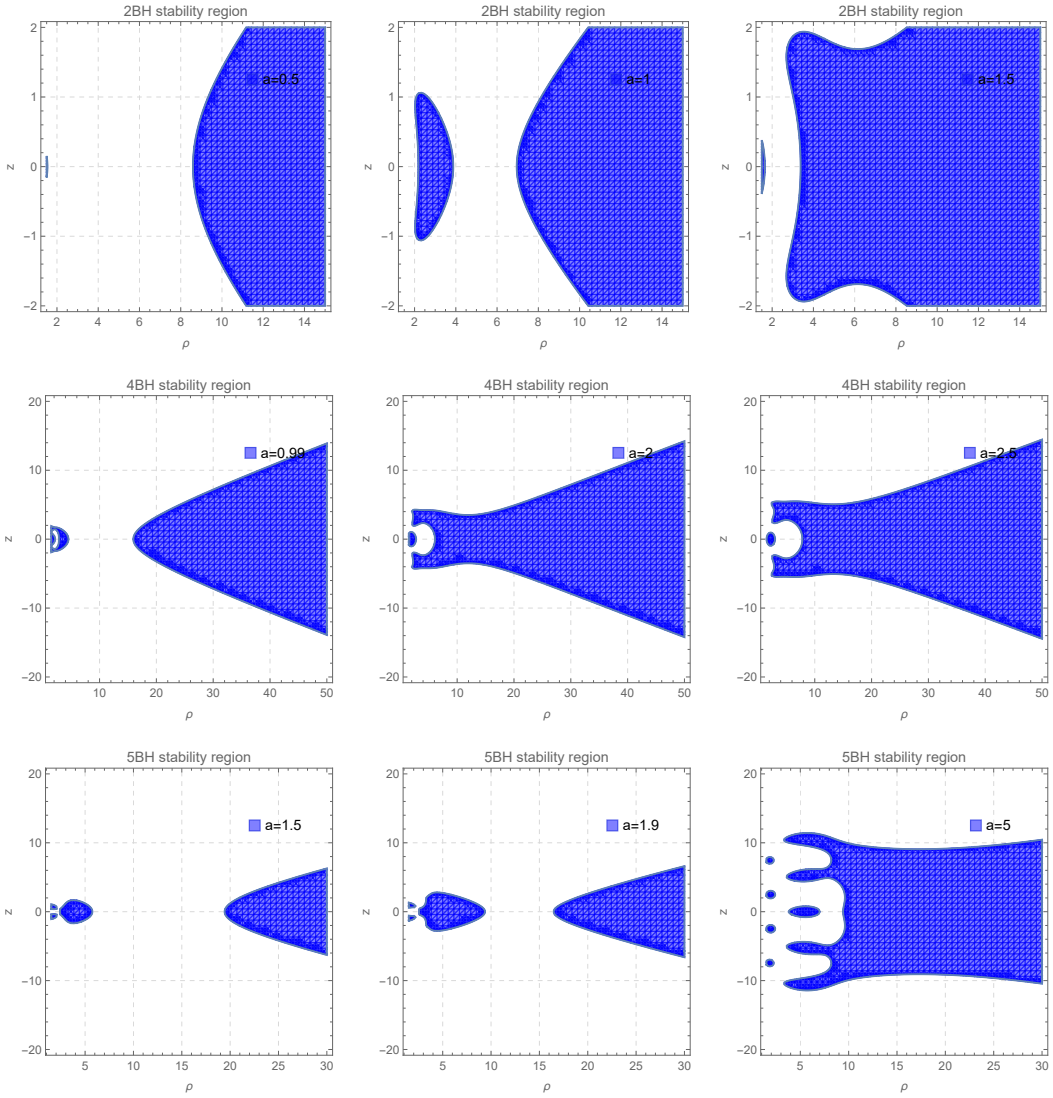

Figure 3. Regions of circular orbital stability in different black hole spacetimes.

4. One-Dimensional Effective Potential Analysis

To study this phenomenon further, we take the example of a TBH spacetime and analyse its one-dimensional effective potential. From Equation (25), it can be introduced that

$$V\left(\rho, z; L^2\right) = \frac{L^2}{\rho^2 U^4} + \frac{1}{U^2}. \tag{33}$$

Letting $z = 0$, $L = 30$, we choose $a = 0.9, 1, 1.1$ for plotting, and we can obtain the one-dimensional effective potential as a function of ρ. As shown in Figure 4, we can clearly see that the one-dimensional effective potential has a bimodal structure, resembling a potential energy well, which is very helpful for us in order to study the properties of multi-static black holes.

To further investigate the one-dimensional effective potential when the separation distance $a = 1$, $L = 20$, we take different values of z and find that the image of the one-dimensional effective potential has a bimodal structure only when $z = 0$, as shown in Figure 5.

Next, with the separation distance set at $a = 1$, we alter the mass ratio of the three black holes by changing the mass of M_3, and we observe that the bimodal structure of the one-dimensional effective potential becomes increasingly pronounced as M_3 increases, as shown in Figure 6.

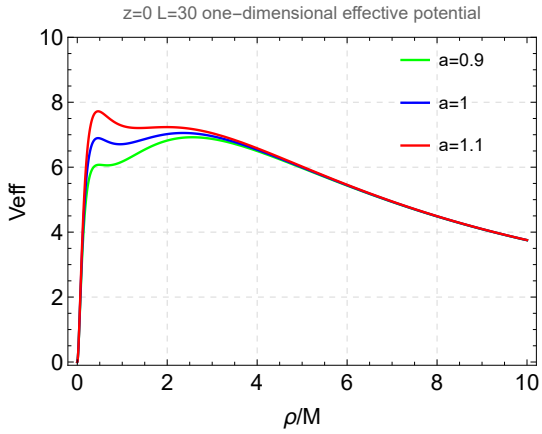

Figure 4. One-dimensional effective potential for different values of the separation distance a.

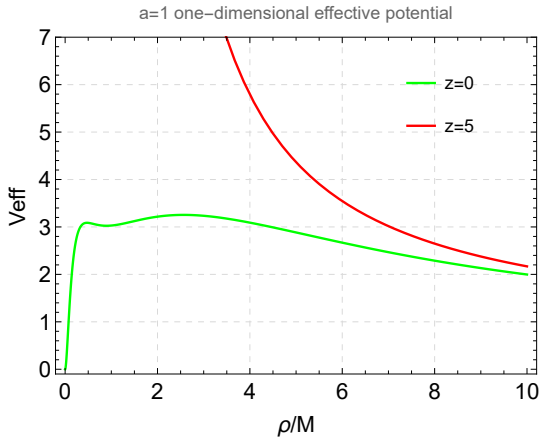

Figure 5. One-dimensional effective potential for different values of z.

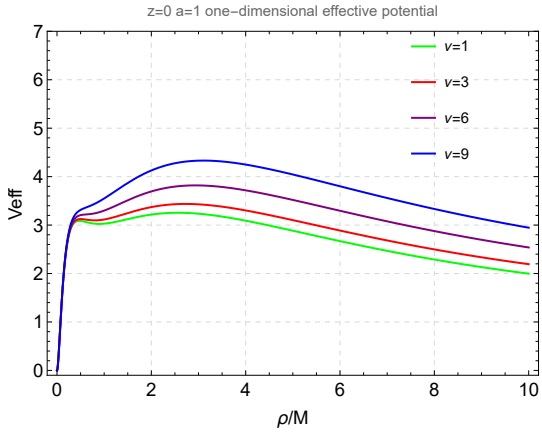

Figure 6. One-dimensional effective potential at different mass ratios when the separation distance $a = 1$.

To further investigate the bi-peak structure of the one-dimensional effective potential, we vary the value of the angular momentum L and find that the larger the angular momentum, the larger the effective potential. The bimodal structure of the one-dimensional effective potential also becomes more pronounced, as shown in Figure 7.

Similarly, we obtain the figure of the one-dimensional effective potential for other black hole spacetimes. As shown in Figure 8.

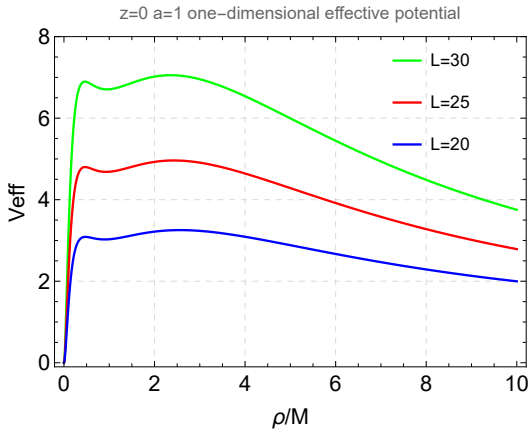

Figure 7. One-dimensional effective potential at different angular momentum L.

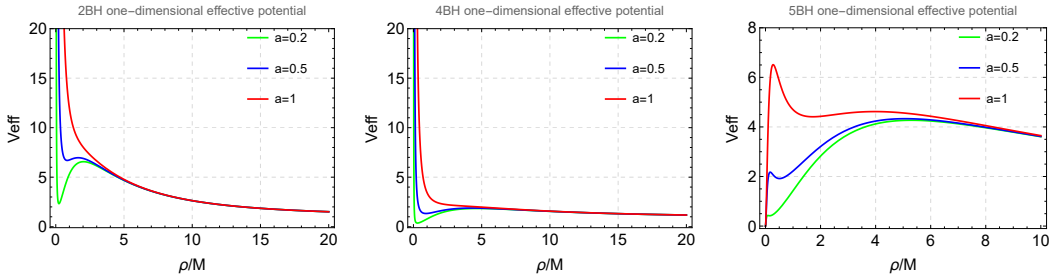

Figure 8. One-dimensional effective potential for two black holes, four black holes, and five black holes.

We find that when the number of black holes is even, the effective potential becomes progressively smaller with distance from infinity and, importantly, the bimodal structure of the one-dimensional effective potential can only be seen when the number of black holes is odd.

5. Three Fundamental Frequencies in Equatorial Circular Orbit in Multi-Static Black Hole Spacetimes

The equatorial circular orbit is described by three fundamental frequencies: (1) Orbital frequency ν_ϕ: This frequency characterizes the circular orbit of an object in the black hole's equatorial plane. It is proportional to the object's angular velocity as it orbits the black hole. (2) Radial local frequency ν_ρ: This frequency represents the object's radial oscillations, which occur perpendicular to the orbital plane and affect the distance between the object and the black hole. It corresponds to the rate at which the object moves radially, reflecting its oscillatory motion within the black hole's gravitational potential well. (3) Vertical local frequency ν_z: This describes the frequency of an object's motion in the longitudinal direction and refers to the frequency at which the object oscillates above and below the equatorial plane of the black hole.

Now let us see how the fundamental frequencies ν_ϕ, ν_ρ, and ν_z can be calculated. Take the frequency projection of a static TBH as an example. The derivation of the orbital frequency requires the geodesic equation to be written first:

$$\frac{\mathrm{d}}{\mathrm{d}\tau}\left(g_{\mu\nu}\dot{x}^\nu\right) = \frac{1}{2}\left(\partial_\mu g_{\nu\rho}\right)\dot{x}^\nu\dot{x}^\rho. \tag{34}$$

For equatorial circular orbits, $\dot{\rho} = \dot{z} = \ddot{\rho} = 0$. In this case, the above equation reduces to

$$\left(\partial_\rho g_{tt}\right)\dot{t}^2 + \left(\partial_\rho g_{\phi\phi}\right)\dot{\phi}^2 = 0, \tag{35}$$

Angular velocity of orbit $\Omega = \dot{\phi}/\dot{t}$:

$$\Omega_{\pm} = \pm\sqrt{-\left(\partial_\rho g_{tt}\right)/\left(\partial_\rho g_{\phi\phi}\right)}. \tag{36}$$

For the calculation of the radial and vertical local frequencies, we proceed as follows. In the linear category, small perturbations in the radial and vertical directions around the equatorial circular orbit can be considered independently. In the context of radial motion, assume that $\dot{z} = 0$, and write $\dot{\rho} = \dot{t}(\,\mathrm{d}\rho/\mathrm{d}t)$.

$$\left(\frac{\mathrm{d}\rho}{\mathrm{d}t}\right)^2 = \frac{1}{g_{\rho\rho}\dot{t}^2} V_{\mathrm{eff}}, \tag{37}$$

Deriving (37) for the coordinate t, we obtain

$$\frac{\mathrm{d}^2\rho}{\mathrm{d}t^2} = \frac{1}{2}\frac{\partial}{\partial\rho}\left(\frac{1}{g_{\rho\rho}\dot{t}^2} V_{\mathrm{eff}}\right) = \frac{V_{\mathrm{eff}}}{2}\frac{\partial}{\partial\rho}\left(\frac{1}{g_{\rho\rho}\dot{t}^2}\right) + \frac{1}{2g_{\rho\rho}\dot{t}^2}\frac{\partial V_{\mathrm{eff}}}{\partial\rho}. \tag{38}$$

Assuming that there is a small displacement near the orbit, $\rho = \rho_0 + \delta_\rho$, one has

$$\frac{\mathrm{d}^2\rho}{\mathrm{d}t^2} = \frac{\mathrm{d}^2\delta_\rho}{\mathrm{d}t^2}, \tag{39}$$

$$V_{\mathrm{eff}}\left(\rho_0 + \delta_\rho\right) = V_{\mathrm{eff}}\left(\rho_0\right) + \left(\frac{\partial V_{\mathrm{eff}}}{\partial\rho}\right)_{\rho=\rho_0}\delta_\rho + O\left(\delta^2\rho\right), \tag{40}$$

$$\left(\frac{\partial V_{\mathrm{eff}}}{\partial\rho}\right)_{\rho=\rho_0+\delta_\rho} = \left(\frac{\partial V_{\mathrm{eff}}}{\partial\rho}\right)_{\rho=\rho_0} + \left(\frac{\partial^2 V_{\mathrm{eff}}}{\partial\rho^2}\right)_{\rho=\rho_0} + O\left(\delta^2\rho\right). \tag{41}$$

By the small displacement deviating from the orbit, $z = z_0 + \delta_z$, the expression in z coordinate is obtained and the high-order small quantity is ignored, respectively. The following differential equation is obtained:

$$\frac{\mathrm{d}^2\delta_\rho}{\mathrm{d}t^2} + \Omega_\rho^2\delta_\rho = 0. \tag{42}$$

$$\frac{\mathrm{d}^2\delta_z}{\mathrm{d}t^2} + \Omega_z^2\delta_z = 0. \tag{43}$$

In the cylindrical coordinate, from Equations (36), (42), and (43), the three fundamental angular velocities are

$$\Omega_\rho^2 = -\frac{1}{2g_{\rho\rho}\dot{t}^2}\frac{\partial^2 V_{\mathrm{eff}}}{\partial\rho^2}, \tag{44}$$

$$\Omega_z^2 = -\frac{1}{2g_{zz}\dot{t}^2}\frac{\partial^2 V_{\mathrm{eff}}}{\partial z^2}, \tag{45}$$

$$\Omega_\phi^2 = -\left(\partial_\rho g_{tt}\right)/\left(\partial_\rho g_{\phi\phi}\right). \tag{46}$$

Therefore, we obtain

$$\nu_\rho = \sqrt{-\frac{1}{2g_{\rho\rho}\dot{t}^2}\frac{\partial^2 V_{\mathrm{eff}}}{\partial\rho^2}}/2\pi, \tag{47}$$

$$\nu_z = \sqrt{-\frac{1}{2g_{zz}\dot{t}^2}\frac{\partial^2 V_{\mathrm{eff}}}{\partial z^2}}/2\pi, \tag{48}$$

$$\nu_\phi = \sqrt{-\left(\partial_\rho g_{tt}\right)/\left(\partial_\rho g_{\phi\phi}\right)}/2\pi. \tag{49}$$

Through Equations (47)–(49), in the plane of $z = 0$, let $a = 0$, so as to obtain the image of coincident orbital frequency and vertical local frequency, which is similar to the case of the Schwarzschild black hole. We draw a diagram of three fundamental frequencies, as shown in Figure 9.

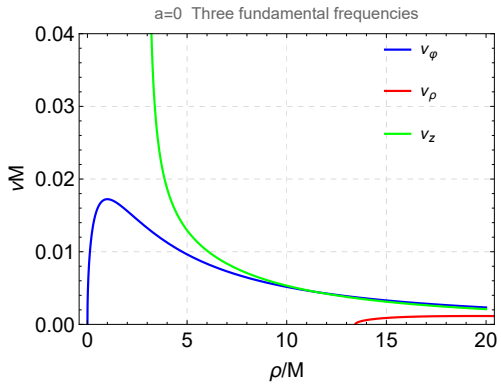

Figure 9. Three fundamental frequencies of a three-black-hole spacetime when $a = 0$.

In Figure 9, we can see that the orbital frequency and the vertical local frequency basically coincide in the second half.

By means of Figure 10, we can find that the radial local frequency is discontinuous, while its intermittent interval coincides exactly with the intermittent interval of the stabilisation region at $a = 1.5$ in Figure 2.

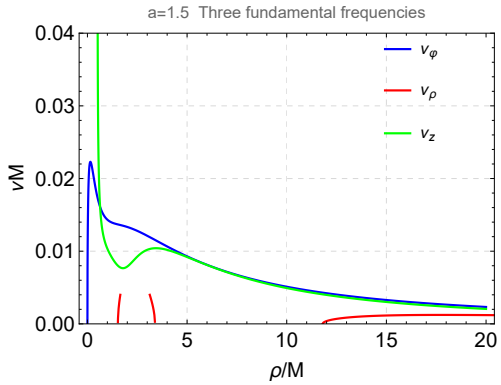

Figure 10. Three fundamental frequencies of a three-black-hole spacetime when $a = 1.5$.

Figure 11 shows us that the orbital frequencies also have a bimodal structure when $a = 1$, which is the same as in the figure of the one-dimensional effective potential.

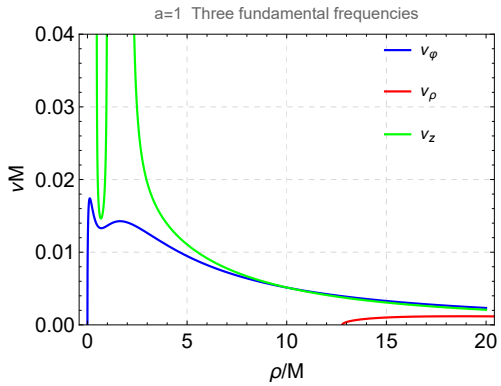

Figure 11. Three fundamental frequencies of a three-black-hole spacetime when $a = 1$.

Again, we can obtain the three fundamental frequencies of the two black holes as a comparison.

As shown in Figure 12, we obtain the three fundamental frequencies of the double-black-hole spacetime, where the orbital and vertical local frequencies essentially coincide in the second half of the image, thus once again verifying that the case $a = 0$ is correct.

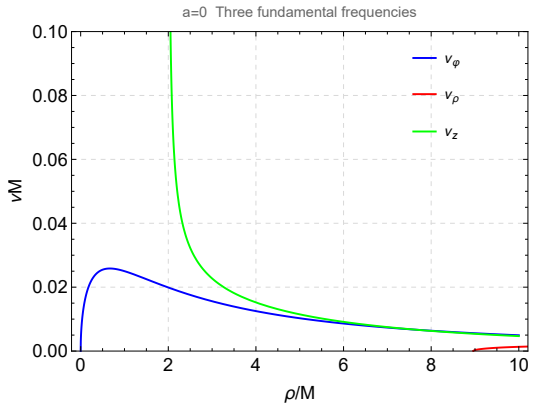

Figure 12. The three fundamental frequencies of the two-black-hole spacetime when $a = 0$.

Next, we explored the frequency variation when $a = 1$ and obtained Figure 13. As expected, the discontinuity interval of the radial local frequency again matches exactly the discontinuity interval at $a = 1$ for the double-black-hole spacetime in Figure 3. This reflects the nature of spacetime and also indicates that the frequencies are closely related to the stability of circular orbits.

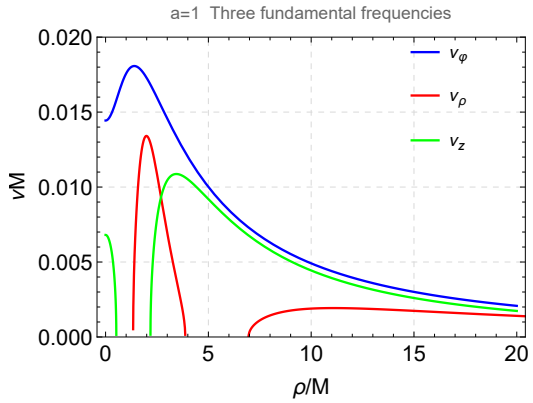

Figure 13. The three fundamental frequencies of the two-black-hole spacetime when $a = 1$.

6. Summary and Discussion

We study stable circular orbits in a static black hole spacetime of the Majumdar–Papapetrou type with equal unit mass, and we consider the circular orbital sequences of test particles in a static black hole spacetime. By comparing the circular orbits of two, three, four and five static black holes at different spacetime scales, we find that the continuity of their stable circular orbits on the equatorial plane changes, that is, the peak of the effective potential changes from a single peak to a bimodal structure, and the distance a between the black holes is the main reason for this change. This feature is completely different from the continuity of the stable circular orbital intervals of any black hole found in the past. We further plot the one-dimensional effective potential of different spacetimes, and find that the parity of the number of black holes has an important effect on the effective potential. We also analyse the effect of the black hole spacing a on the three fundamental frequencies of the circular orbit, and compare the three fundamental frequencies in two and three static black hole spacetimes. An important finding is that when the distance a changes, the

continuity of the fundamental orbital frequency synchronizes with the continuity of the ISCO, indicating a close correlation between these two physical quantities.

We highlight the significance of orbital frequency. For example, under certain conditions, the radial frequency may become zero, meaning that the orbit may become unstable and the object may fall into a black hole or be thrown out to infinity. Under certain conditions, resonance phenomena can occur between these frequencies, leading to complex orbital behaviour. This is important for understanding high-energy astrophysical phenomena around black holes. The orbital fundamental frequency is an important parameter for analysing gravitational wave radiation. When an object orbits a black hole, it emits gravitational waves at frequencies that are tied to these three fundamental frequencies. Consequently, comprehending these frequencies is instrumental in forecasting and examining the gravitational wave emissions from black hole systems. Knowledge of these frequencies helps to explain some observed astrophysical phenomena, such as the characterisation of black holes in X-ray binary systems, and the radiation mechanism of active galactic nuclei. Overall, the three orbital fundamental frequencies in the black hole spacetime provide crucial information to understand and characterise the laws of motion of celestial bodies in strong gravitational fields and have a wide range of applications in astrophysics and gravitational wave astronomy.

We present a systematic approach to finding stationary orbits and suggest methods for determining whether these orbits are stable or unstable. Using these methods, we identify a typical sequence of circular orbits for each model and indicate the parts of them that exhibit stable behaviour. These orbits are balanced by Newtonian gravity and centrifugal forces. Stabilised circular orbits can also be balanced by other mechanisms. Like the familiar Schwarzschild black hole, particles near the event horizon experience higher-order relativistic effects. Conversely, due to the absence of an event horizon on the symmetry plane of this evenly static black hole spacetime, the centrifugal barrier experienced by particles necessarily tends towards infinity at the centre. As a result, a stable equilibrium point arises radially, achieved through the balance of higher-order relativistic gravitational and centrifugal forces. Furthermore, if this point is also located in a vertically bounded region, a stable circular orbit emerges. And this region of stability of the circular orbit is tied to the three orbital fundamental frequencies, which is very common for a spacetime where there is no horizon at the centre of the system.

This model does not fully reflect real astrophysical conditions, particularly the impact of black hole spin on ISCO and orbit stability. The stability of multi-black hole systems is uncertain. The effects of spin on spacetime are complex, influencing orbit frequencies and Lagrange points. Dark matter halos are also a focus, altering the gravitational potential and influencing ISCO positions and orbit stability. The presence of dark matter can change the effective potential's shape, affecting orbital stability and fundamental frequencies. Further research is needed to fully understand these complex interactions. While these effects are currently unknown, we plan to explore them in future work. The study of these changes will lead to a better understanding of the distribution and nature of dark matter in the Universe and its potential impact on astrophysical phenomena.

Author Contributions: Conceptualisation, Z.F., Y.W. and X.W.; methodology, Y.W.; software, Z.F.; validation, Y.W. and Z.F.; formal analysis, Y.W.; investigation, Y.W.; resources, Z.F.; data curation, Z.F.; writing—original draft preparation, Z.F.; writing—review and editing, Z.F., Y.W. and X.W.; visualisation, Y.W.; supervision, Y.W.; project administration, X.W.; funding acquisition, X.W. All authors have read and agreed to the published version of the manuscript.

Funding: This work is supported by the National Natural Science Foundation of China (grant Nos. 12373042 and U1938201), the Bagui Scholars Programme (W.X.-G.).

Data Availability Statement: Data are contained within the article.

Conflicts of Interest: The authors declare no conflicts of interest.

References

1. Abbott, B.P.; Abbott, R.; Abbott, T.; Abraham, S.; Acernese, F.; Ackley, K.; Adams, C.; Adhikari, R.; Adya, V.; Affeldt, C.; et al. GWTC-1: A gravitational-wave transient catalog of compact binary mergers observed by LIGO and Virgo during the first and second observing runs. *Phys. Rev.* **2019**, *9*, 031040. [CrossRef]
2. Abbott, B.P.; Abbott, R.; Abbott, T.; Abernathy, M.; Acernese, F.; Ackley, K.; Adams, C.; Adams, T.; Addesso, P.; Adhikari, R.X.; et al. Observation of gravitational waves from a binary black hole merger. *Phys. Rev. Lett.* **2016**, *116*, 061102. [CrossRef] [PubMed]
3. Abbott, B.P.; Abbott, R.; Abbott, T.; Abernathy, M.; Acernese, F.; Ackley, K.; Adams, C.; Adams, T.; Addesso, P.; Adhikari, R.; et al. Properties of the binary black hole merger GW150914. *Physical Rev. Lett.* **2016**, *116*, 241102.
4. Nakashi, K.; Igata, T. Innermost stable circular orbits in the Majumdar-Papapetrou dihole spacetime. *Phys. Rev. D* **2019**, *99*, 124033. [CrossRef]
5. Imbrogno, M.; Meringolo, C.; Servidio, S. Strong interactions in the three black holes problem. *arXiv* **2021**, arXiv:2108.01392.
6. Galaviz, P.; Brügmann, B. Characterization of the gravitational wave emission of three black holes. *Phys. Rev. D* **2011**, *83*, 084013. [CrossRef]
7. Veske, D.; Márka, Z.; Sullivan, A.G.; Bartos, I.; Rainer Corley, K.; Samsing, J.; Márka, S. Have hierarchical three-body mergers been detected by LIGO/Virgo? *Mon. Not. R. Astron. Soc. Lett.* **2020**, *498*, L46–L52. [CrossRef]
8. Hao, W.; Kouwenhoven, M.; Spurzem, R.; Amaro-Seoane, P.; Mardling, R.A.; Xu, X. Analysis of Kozai cycles in equal-mass hierarchical triple supermassive black hole mergers in the presence of a stellar cluster. *Mon. Not. R. Astron. Soc.* **2024**, *527*, 10705–10725. [CrossRef]
9. Liu, X.; Hou, M.; Li, Z.; Nyland, K.; Guo, H.; Kong, M.; Shen, Y.; Wrobel, J.M.; Peng, S. A Trio of Massive Black Holes Caught in the Act of Merging. *Astrophys. J.* **2019**, *887*, 90. [CrossRef]
10. Galaviz, P.; Bruegmann, B.; Cao, Z. Numerical evolution of multiple black holes with accurate initial data. *Phys. Rev. D* **2010**, *82*, 024005. [CrossRef]
11. Fragione, G.; Kocsis, B.; Rasio, F.A.; Silk, J. Repeated mergers, mass-gap black holes, and formation of intermediate-mass black holes in dense massive star clusters. *Astrophys. J.* **2022**, *927*, 231. [CrossRef]
12. Veske, D.; Sullivan, A.G.; Márka, Z.; Bartos, I.; Corley, K.R.; Samsing, J.; Buscicchio, R.; Márka, S. Search for black hole merger families. *Astrophys. J. Lett.* **2021**, *907*, L48. [CrossRef]
13. Ficarra, G.; Ciarfella, A.; Lousto, C.O. Close encounter of three black holes revisited. *Phys. Rev. D* **2023**, *108*, 064045. [CrossRef]
14. Campanelli, M.; Dettwyler, M.; Hannam, M.; Lousto, C.O. Relativistic three-body effects in black hole coalescence. *Phys. Rev. D* **2006**, *74*. [CrossRef]
15. Torigoe, Y.; Hattori, K.; Asada, H. Gravitational waveforms for 2 and 3-body gravitating systems. *Phys. Rev. Lett.* **2009**, *102*, 251101. [CrossRef] [PubMed]
16. Seto, N. Relativistic Resonant Relations between Massive Black Hole Binary and Extreme Mass Ratio Inspiral. *Phys. Rev. D* **2012**, *85*, 064037. [CrossRef]
17. Yamada, K.; Asada, H. Nonchaotic evolution of triangular configuration due to gravitational radiation reaction in the three-body problem. *Phys. Rev. D* **2016**, *93*, 084027. [CrossRef]
18. Hayasaki, K.; Mineshige, S.; Sudou, H. Binary Black Hole Accretion Flows in Merged Galactic Nuclei. *Publ. Astron. Soc. Jap.* **2007**, *59*, 427. [CrossRef]
19. Kimitake, H.; Mineshige, S.; Ho, L.C. A supermassive binary black hole with triple disks. *Astrophys. J.* **2008**, *682*, 1134. [CrossRef]
20. Clark, J.P.A.; Eardley, D.M. Evolution of close neutron star binaries. *Astrophys. J.* **1977**, *215*, 311–322. [CrossRef]
21. Kidder, L.E.; Will, C.M.; Wiseman, A.G. Coalescing binary systems of compact objects to (post)**(5/2)-Newtonian order. 3. Transition from inspiral to plunge. *Phys. Rev. D* **1993**, *47*, 3281–3291. [CrossRef] [PubMed]
22. Cao, Z.; Yu, J.P.; Lin, C.Y.; Bai, S.; Yo, H.J. Perturbational Treatment of the Gravitational Potential Effect on Binary Black Hole Evolution. *J. Phys. Conf. Ser.* **2012**, *330*, 012016.
23. Weyl, H. The theory of gravitation. *Annalen Phys.* **1917**, *54*, 117–145. [CrossRef]
24. Majumdar, S.D. A class of exact solutions of Einstein's field equations. *Phys. Rev.* **1947**, *72*, 390–398. [CrossRef]
25. Papaetrou, A. A Static solution of the equations of the gravitational field for an arbitrary charge distribution. *Proc. Roy. Irish Acad. A* **1947**, *51*, 191–204.
26. Kramer, D.; Neugebauer, G. The superposition of two Kerr solutions. *Phys. Lett.* **1980**, *75*, 259–261. [CrossRef]
27. Tomizawa, S.; Igata, T. Stable circular orbits in Kaluza-Klein black hole spacetimes. *Phys. Rev. D* **2021**, *103*, 124004. [CrossRef]
28. Igata, T.; Tomizawa, S. Stable circular orbits in caged black hole spacetimes. *Phys. Rev. D* **2021**, *103*, 084011. [CrossRef]
29. Schroven, K.; Grunau, S. Innermost stable circular orbit of charged particles in Reissner-Nordström, Kerr-Newman, and Kerr-Sen spacetimes. *Phys. Rev. D* **2021**, *103*, 024016. [CrossRef]
30. Igata, T.; Tomizawa, S. Stable circular orbits in higher-dimensional multi–black-hole spacetimes. *Phys. Rev. D* **2020**, *102*, 084003. [CrossRef]
31. Nakashi, K.; Igata, T. Effect of a second compact object on stable circular orbits. *Phys. Rev. D* **2019**, *100*, 104006. [CrossRef]
32. Al Zahrani, A.M. Tilted circular orbits around a Kerr black hole. *Phys. Rev. D* **2024**, *109*, 024029. [CrossRef]
33. Suzuki, R.; Tomizawa, S. Stable bound orbits around static Einstein-Gauss-Bonnet black holes. *Phys. Rev. D* **2022**, *105*, 124033. [CrossRef]

34. Shen, G.; Wang, Y.; Lü, H. Space-Time Properties of Extreme RN Black Holes in Static Triangular Distribution. *Symmetry* **2023**, *15*, 505. [CrossRef]
35. Wang, Y.; Shen, G.; Sun, X. The Space-Time Properties of Three Static Black Holes. *Symmetry* **2023**, *15*, 702. [CrossRef]
36. Balali, A.E. Quantum Schwarzschild Black Hole Optical Aspects. [CrossRef]
37. Hartle, J.B.; Hawking, S.W. Solutions of the Einstein-Maxwell equations with many black holes. *Commun. Math. Phys.* **1972**, *26*, 87–101. [CrossRef]